Journal of Non-Crystalline Solids 404 (2014) 124–134

Contents lists available at ScienceDirect

Journal of Non-Crystalline Solids

journal homepage: www.elsevier.com/ locate/ jnoncrysol

Strain-rate sensitivity of glasses

Rene Limbach, Bruno P. Rodrigues, Lothar Wondraczek *

Otto Schott Institute of Materials Research, University of Jena, Fraunhoferstrasse 6, 07743 Jena, Germany

ARTICLE INFO

Article history:
Received 20 June 2014
Received in revised form 7 August 2014
Available online 30 August 2014

Keywords:
Glass;
Plasticity;
Hardness;
Strain-rate sensitivity;
Mechanical properties;
Deformation

ABSTRACT

We report on the loading-rate dependence of localized plastic deformation in inorganic covalent, metallic, ionic and superionic glasses. For this, the strain-rate sensitivity is determined through instrumented nanoindentation in a load-controlled strain-rate jump test. Through relating the strain-rate sensitivity to the reduced temperature, the packing density, the network dimensionality and the average single bond strength of the system, a qualitative mechanistic description of the strain-mediating process is possible. A strong variability of strain-rate sensitivity is obtained only at intermediate values of packing density, network connectivity or bond strength, when other parameters such as chemical composition and specific structural arrangement are dominating the deformation process. On the other side, for high bond strength and connectivity or for high packing density, the strain-rate sensitivity of the considered glasses is always low, which is also confirmed through the dependence of strain-rate sensitivity on Poisson ratio. Here, only for glasses with a Poisson ratio of ~0.3–0.4 we observe a wide variability of the loading-rate dependence of local deformation. For higher or lower Poisson ratio, the observed dependence is always low: when the limiting factor in deformation is primarily network connectivity and bond strength or packing density, respectively, once an activation barrier is overcome, deformation is only weakly loading-rate-dependent. This is regardless of the height of the activation barrier. When approaching the glass transition temperature, high strain-rate sensitivity is observed only in glasses where non-Newtonian flow is expected also in the corresponding liquid.

1. Introduction

Glasses are among the – theoretically – strongest man-made materials. However, practical use of the very high levels of intrinsic strength is largely limited by their brittleness and sensitivity to surface damage, i.e., by their ability to resist the generation and growth of mechanical defects [1]. The phenomenological formalism of *hardness* has often been used to describe this behavior. Thereby, various definitions of hardness exist, all of them more or less relating to the material's ability to resist penetration of a sharp object. What came as a surprise originally was that such penetration is driven by plastic deformation [2], even in materials which have otherwise been thought-of as ideally brittle. Different experimental approaches are now being used to quantify *hardness*, such as observing the penetration of Vickers, Berkovich or sharp cube-corner indenters into the material's surface, and efforts are being made to relate such observations to application-related glass properties like brittleness [3], scratch-resistance [4] or toughness [5]. On the other hand, the very complex mechanisms that underlie the phenomenon of glass hardness remain poorly understood. This is an inherent result of the way in which hardness is determined: The visible resistance against the penetration of an indenter may result from a convolution of various related and un-related processes. Yamane and Mackenzie [6] have roughly separated this phenomenology into three contributions, i.e., elastic deformation, densification and plastic flow. A distinction is sometimes (partially) possible through relaxation experiments on post-mortem (as-indented) samples [7–9].

In recent years, *nano*indentation has become an effective tool to investigate the mechanical properties of surface layers in small tested volumes [10–13]. Due to the low loads which are typically applied in such experiments, indentation cracking is usually avoided. In a first approximation, the method relies on the assumption that time-dependent effects in the analysis of the load–displacement curve can be neglected [12–16]. Nonetheless, most materials show some form of time-dependent plastic deformation under stress [15–18], which may manifest in an indentation size effect (i.e., increasing hardness with decreasing penetration depth [19]) or in a strain-rate dependence of hardness [20].

2. Strain-rate dependence of glass hardness

To investigate the influence of the time-dependent plastic deformation during an indentation test, Chu and Li [21] introduced an impression creep test in which an indenter was pushed into a sample with a constant velocity until a predefined load was reached. Then, the load was fixed and the progressive sink-in of the indenter was monitored over time. During this process, the subjacent elastic–plastic half

* Corresponding author. Tel.: +49 3641 948500.
E-mail address: lothar.wondraczek@uni-jena.de (L. Wondraczek).

http://dx.doi.org/10.1016/j.jnoncrysol.2014.08.023

space expands into the surrounding, previously undeformed material [22–24], whereas a secondary steady-state creep regime is assumed to be present inside the plastically deformed volume [24–27].

The impression creep test was originally used in the study of metals as a practical alternative to the uniaxial tensile test, since the latter cannot easily be performed on very small volumes [23,28,29]. In metals, the time-dependent plastic deformation is based on the diffusion of atoms or on the movement of dislocations [16,18,21,30]. On the other hand, the time-dependent plastic deformation in glasses is commonly thought to be determined by viscous flow [18,22,31]. This assumption may be somewhat oversimplified if we consider in more detail how a hypothetic glass may accommodate the penetration of a hard indenter. This is illustrated schematically in Fig. 1. For simplicity, we assume an initially ordered, simple cubic matrix of atoms (Fig. 1a). Fig. 1b–e shows the reaction paths over which the local structure may rearrange in principle to compensate the penetrating volume. In the first step of this consideration, we disregard the question of elasticity and reversibility, but extend the classical view of Yamane and Mackenzie [6] through a structural component: in the simplest case, the considered material may densify congruently, i.e., by a reduction of the interatomic distances without any displacive or reconstructive reactions (e.g., low pressure reactions of various silicate glasses [32], Fig. 1b). A second possibility is a change in the coordination environment (usually an increase in coordination number). This leads to more dense local packing (Fig. 1c), a scenario that has been observed, e.g., in borosilicate glasses [33–35]. Thirdly, the already noted viscous flow may be considered, which would be strongly time-dependent (Fig. 1d). A final option is the generation of shear bands (Fig. 1e). In reality, a mixed scenario is most probable, e.g., where congruent densification is followed by structural rearrangements and shear (suggested in, e.g., vitreous B_2O_3 and borate glasses [36,37]).

Generally, in a *uniaxial* tensile creep test, the creep stress σ is related to a steady-state creep rate $\dot{\varepsilon}$ through a simple power-law of the form [24–26]:

$$\dot{\varepsilon} = K \cdot \sigma^{n} = K \cdot \sigma^{1/m} \tag{1}$$

, where the pre-exponential factor K is a material-dependent parameter and the exponents n and m are the stress exponent and the strain-rate sensitivity, respectively.

From Eq. (1), it can be seen that the strain-rate sensitivity of a material describes the non-linear dependence of the deformation rate on the applied stress, similar to, e.g., a deviation from Newtonian flow of a liquid. It must be clearly understood for the following argument that it is not a measure of the material's softness or plasticity.

Earlier investigations performed by Tabor [38] had shown that the mean contact pressure under an indenter tip, defined as the hardness of the material, can be transformed into a flow stress σ_r at a representative strain ε_r by using the constraint factor *c*:

$$H = c \cdot \sigma_r(\varepsilon_r) \tag{2}$$

For metals and alloys with a negligible amount of elastic deformation, it is c ~ 3, whereas for brittle materials, where the deformation is primary elastic, *c* is smaller, c < 3, depending on the elastic properties of the system [27,38–40].

With the further assumption of a steady-state creep regime below the indenter tip, the indentation strain-rate $\dot{\varepsilon}_i$ in an impression creep test can be derived from the time-derivate of the indentation depth dh/dt divided by the actual displacement h according to [24]:

$$\dot{\varepsilon}_i = \left(\frac{1}{h}\right)\frac{dh}{dt} = \frac{\dot{h}}{h} \tag{3}$$

and by combining Eqs. (1)–(3) the strain-rate sensitivity of the hardness is defined as:

$$n = \frac{\ln \dot{\varepsilon}_i}{\ln H} = \frac{1}{m} \tag{4}$$

In the above equation, a value of m = 0 describes a rigid-perfectly plastic material and m = 1 stands for a linear viscous solid, respectively [41,42].

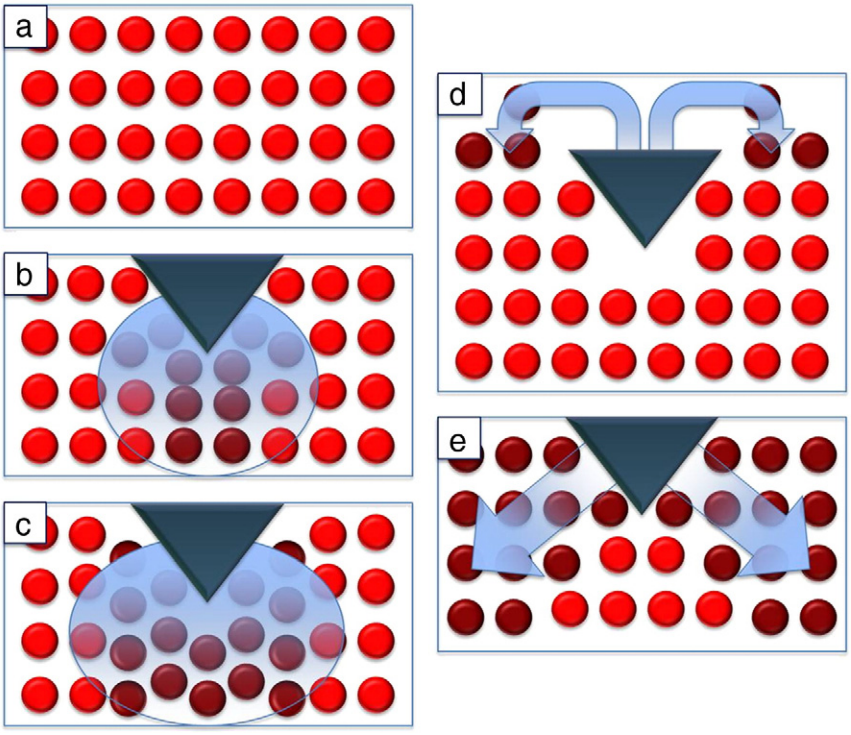

Fig. 1. Schematic paths of structural rearrangement in reaction to a penetrating volume. (a) Simplified case of a simple cubic lattice; (b) congruent densification in the indenter zone; (c) increasing coordination number; (d) viscous flow and pile-up; (e) deformation through shear band formation.

While a number of studies on metals, alloys and ceramics showed good agreement between the impression creep tests and the uniaxial tensile tests [23,28,29,43,44], the former method is not suitable to investigate the rate-dependent plastic deformation of brittle glasses as it occurs in a conventional indentation test. It is well known that most inorganic glass-forming materials behave like a Newtonian fluid at temperatures above the glass transition and at moderate deformation rate [45–49]. For a Newtonian fluid, the stresses are proportional to the applied strain-rates, with the viscosity being the proportionality constant [49–52]. Based on this relation the viscosity was determined by an indentation creep test for a variety of glass systems at temperatures around their glass transition range [51–59]. However, the application of sufficiently high stresses or strain-rates can lead to a change from the linear Newtonian viscous flow to an inhomogeneous or non-Newtonian viscous flow with a reduction (or increase) of the apparent shear viscosity [46–50,60]. It is assumed that a similar mechanism is responsible for the rate dependence of plastic deformation of glasses during an indentation test [22,31,55,58].

To overcome this problem, an indentation test with constant strain-rate can be applied where the strain-rate $\dot{\varepsilon}$ (expressed as the loading-rate divided by the actual load $\dot{P}/P$) is kept constant over the whole indentation depth, with the consequence that for a homogenous material with a depth-independent hardness, a steady-state stress regime is formed below the indenter tip after a certain displacement is reached [18,23,26]. By this means, the rate-dependent plastic deformation of a specimen can be investigated at high stress and high strain-rate [24,25]. In addition, the influence of thermal drift is considerably smaller compared to an impression creep test. Creep exponents which have been determined for metals in this way were found to be in good accordance with the uniaxial tensile test results [23,61,62].

In the present study, we investigate the strain-rate sensitivity of glasses over a broad range of compositions, including covalent, metallic, ionic and superionic glasses. As a first objective, the strain-rate dependence of the hardness is determined by a modified constant strain-rate nanoindentation test procedure with strain-rate jumps. Secondly, we correlate the results with thermo-physical and structural properties, such as the atomic packing density, the network dimensionality and the average single bond strength, in order to obtain a mechanistic view at the rate dependence of the surface deformation processes in glasses.

3. Experimental

3.1. Sample preparation

Most glasses on which we report in this study were prepared by conventional melt-quenching techniques, except for Suprasil (Heraeus) and Corning 7980 (Corning) fused silica, respectively, which were received from the manufacturers. Compositions together with some selected physical and mechanical properties are listed in Table 1. Detailed information on the preparation of the M_2O–B_2O_3–SiO_2 (M = Li, Na) and Na_2O–CaO–SiO_2 [34], ZnO–M_2O–SO_3–P_2O_5 (M = Li, Na, Rb, Ag) [63], MO–B_2O_3 (M = Sr, Mn, Eu) [64], AgO–P_2O_5–AgI [65] and MO–P_2O_5 (M = Ca, Mg, Sr) [66] glass series is reported elsewhere.

The densities ρ were measured by the Archimedes method in distilled water and dry ethanol, respectively. Glass transition temperatures T_g were determined by differential scanning calorimetry (DSC).

3.2. Nanoindentation

The mechanical properties were investigated through instrumented indentation testing with a nanoindenter (G200, Agilent Inc.), equipped with a three-sided Berkovich diamond tip and operating in the continuous stiffness measurement (CSM) mode. In this setup, the continuously increasing load–displacement signal is superimposed by weak oscillation of the indenter tip (Δh = 2 nm, f = 45 Hz). This enables parallel determination of hardness H and elastic modulus E as a function of displacement into the surface by continuously recording the indentation depth h, load P and contact stiffness S. The value of *S* corresponds to the initial slope of the unloading load–displacement curve dP/dh.

The results from the nanoindentation experiments were analyzed using the method presented by Oliver and Pharr [12] where H is derived from the load divided by the projected contact area of the indenter tip A_c:

$$H = \frac{P}{A_c} \tag{5}$$

The elastic modulus is obtained from the reduced elastic modulus E_r:

$$E = \left(1-\nu^2\right)\left[\frac{1}{E_r} - \frac{1-\nu_i^2}{E_i}\right]^{-1} \tag{6}$$

, with:

$$E_r = \frac{S}{2\beta}\sqrt{\frac{\pi}{A_c}} \tag{7}$$

Here, E_i, ν_i and ν represent the elastic modulus and the Poisson ratio of the diamond indenter tip (E_i = 1141 GPa, ν_i = 0.07), and the Poisson ratio of the sample. The parameter β in the above equation represents a correction factor [75] that was set to unity for the Berkovich tip used in this study.

Poisson ratios of the borate glasses were determined by Brillouin scattering at the Institut Lumière Materière at the University of Lyon 1, Lyon, France. Values for commercial Suprasil (Heraeus Quarzglas GmbH & Co KG) and Corning 7980 (Corning Inc.) fused silica, respectively, were taken from the corresponding product datasheets and data of silver metaphosphate-silver iodide glasses can be found in the literature [67,68]. The Poisson ratios of the soda-lime silicate, alkali borosilicate, alkaline earth metaphosphate and sulfophosphate glass series were obtained by measuring the longitudinal v_L and transversal sound wave velocities v_T with an Echometer 1077 (Karl Deutsch GmbH & Co. KG):

$$\nu = \frac{v_L^2 - 2v_T^2}{2\left(v_L^2 - v_T^2\right)} \tag{8}$$

For a geometrically self-similar indenter like the three-sided Berkovich tip, the contact area is related to the contact depth h_c through a simple polynomial function of the form:

$$A_c = c_0 h_c^2 + c_1 h_c + c_2 h_c^{1/2} + c_3 h_c^{1/4} + \ldots + c_8 h_c^{1/128} \tag{9}$$

Here, the first term $c_0 h_c^2 = 24.5 h_c^2$ represents the area function of a perfect Berkovich tip. The remaining terms account for deviations from this ideal tip geometry [10,12,76]. The contact depth h_c used in Eq. (8) can be calculated from the load, displacement and the contact stiffness recorded by the CSM module:

$$h_c = h - 0.75\frac{P}{S} \tag{10}$$

Nanoindentation experiments were performed on co-planar, optically polished specimens. Prior to the measurements, the samples were stored in a desiccator and cleaned with ethanol. On each glass sample, 15 indents to a depth of 2 μm were generated at a constant strain-rate of 0.05 s^{-1} and with a 50 μm distance between each indent to avoid the influence of residual stress fields [10]. Values of H and E were recorded as a function of the indentation depth and were averaged between the upper 10% and the lower 20% of each indentation profile. All measurements were carried out in laboratory air under ambient conditions (T = 299 ± 1 K, rH = 28 ± 1%).

Table 1
Physical and mechanical properties of the glasses investigated.

Glass composition	Density	Glass transition	Reduced temperature	Atomic packing density	Poisson ratio	Elastic modulus	Hardness	Strain-rate sensitivity	Average single bond strength
(mol%)	ρ (g/cm^3) ± 0.2%	T_g (K) ± 2 K	T/T_g	C_g	v	E (GPa)	H (GPa)	m	$B_{M\text{-}O}$ (kJ/mol)
SiO_2[a]	2.20	1315	0.23	0.457	0.180	71.8 ± 0.2	9.28 ± 0.05	0.0100	443.7
SiO_2[b]	2.20	1393	0.21	0.447	0.170	71.6 ± 0.3	9.17 ± 0.12	0.0068	443.7
$16Na_2O$–$10CaO$–$74SiO_2$	2.48	803	0.37	0.490	0.221	76.0 ± 0.4	6.67 ± 0.04	0.0164	359.7
$16Na_2O$–$10CaO$–$74SiO_2$ + 500 ppm H_2O	2.48	833	0.36	0.494	0.225	76.8 ± 0.3	6.84 ± 0.04	0.0125	363.3
$16Na_2O$–$10CaO$–$74SiO_2$ + 1000 ppm H_2O	2.48	833	0.36	0.494	0.212	77.4 ± 0.3	6.87 ± 0.05	0.0126	363.4
$16Na_2O$–$10CaO$–$74SiO_2$ + 2000 ppm H_2O	2.48	833	0.36	0.494	0.223	76.6 ± 0.2	6.81 ± 0.07	0.0146	363.5
$12.5Na_2O$–$62.5B_2O_3$–$25.0SiO_2$	2.18	688	0.44	0.539	0.268	41.6 ± 0.2	3.96 ± 0.03	0.0259	418.4
$3.0Na_2O$–$48.5B_2O_3$–$48.5SiO_2$	2.04	653	0.46	0.487	0.257	32.1 ± 0.2	3.68 ± 0.04	0.0270	455.5
$15.0Na_2O$–$42.5B_2O_3$–$42.5SiO_2$	2.31	763	0.39	0.543	0.238	57.1 ± 0.2	5.33 ± 0.03	0.0279	414.8
$6.5Na_2O$–$33.5B_2O_3$–$60.0SiO_2$	2.15	718	0.42	0.493	0.237	44.4 ± 0.1	4.98 ± 0.03	0.0240	456.6
$10Na_2O$–$16B_2O_3$–$74SiO_2$	2.45	823	0.36	0.534	0.204	81.4 ± 0.3	7.26 ± 0.04	0.0211	417.9
$4.3Na_2O$–$20.7B_2O_3$–$74.0SiO_2$–$1.0Al_2O_3$	2.18			0.481	0.210	50.6 ± 0.2	5.89 ± 0.04	0.0209	434.6
$5.4Li_2O$–$1.3Al_2O_3$–$11.8B_2O_3$–$81.5SiO_2$	2.14	762	0.39	0.459	0.201	56.7 ± 0.3	6.96 ± 0.7	0.0149	433.9
$10Na_2O$–$16B_2O_3$–$74SiO_2$	2.45	823	0.36	0.534	0.206	84.4 ± 0.3	7.97 ± 0.05	0.0223	417.9
$42.20ZnO$–$19.79Li_2O$–$19.11SO_3$–$18.90P_2O_5$	3.14	576	0.52	0.522	0.317	63.7 ± 0.6	4.29 ± 0.07	0.0227	268.6
$42.20ZnO$–$19.79Na_2O$–$19.11SO_3$–$18.90P_2O_5$	3.19	579	0.52	0.522	0.303	49.1 ± 0.2	3.43 ± 0.02	0.0204	255.4
$42.20ZnO$–$19.79Rb_2O$–$19.11SO_3$–$18.90P_2O_5$	3.38	621	0.48	0.507	0.294	39.5 ± 0.3	3.02 ± 0.04	0.0281	257.9
$42.20ZnO$–$19.79Ag_2O$–$19.11SO_3$–$18.90P_2O_5$	4.38	558	0.54	0.519	0.369	48.4 ± 0.4	3.59 ± 0.04	0.0229	257.0
$30EuO$–$70B_2O_3$	3.92	911	0.33	0.637	0.286 ± 0.0005	103.7 ± 0.5	8.27 ± 0.05	0.0161	–
$30MnO$–$70B_2O_3$	2.79	857	0.35	0.603	0.291 ± 0.0005	71.8 ± 0.9	6.02 ± 0.16	0.0241	351.5
$30SrO$–$70B_2O_3$	2.80	895	0.33	0.566	0.281 ± 0.0005	82.5 ± 1.3	6.96 ± 0.17	0.0164	364.0
$15EuO$–$15MnO$–$70B_2O_3$	3.30	898	0.33	0.609	0.282 ± 0.0005	88.5 ± 0.7	7.42 ± 0.05	0.0206	–
$15EuO$–$15SrO$–$70B_2O_3$	3.21	894	0.33	0.579	0.280 ± 0.0005	82.0 ± 0.4	6.92 ± 0.04	0.0184	–
$15MnO$–$15SrO$–$70B_2O_3$	2.76	864	0.34	0.576	0.288 ± 0.0005	74.9 ± 0.2	6.34 ± 0.03	0.0160	331.0
$10EuO$–$10MnO$–$10SrO$–$70B_2O_3$	3.07	866	0.34	0.584	0.286 ± 0.0005	80.9 ± 0.3	6.88 ± 0.02	0.0156	–
$50CaO$–$50P_2O_5$	2.65	809	0.37	0.539	0.273	58.6 ± 0.2	4.58 ± 0.03	0.0223	308.1
$12.5MgO$–$37.5CaO$–$50.0P_2O_5$	2.63	808	0.37	0.537	0.265	62.1 ± 0.2	4.90 ± 0.02	0.0208	317.9
$25MgO$–$25CaO$–$50P_2O_5$	2.60	811	0.37	0.538	0.256	65.0 ± 0.2	5.25 ± 0.03	0.0196	327.8

(continued on next page)

Table 1 *(continued)*

Glass composition	Density	Glass transition	Reduced temperature	Atomic packing density	Poisson ratio	Elastic modulus	Hardness	Strain-rate sensitivity	Average single bond strength
(mol%)	ρ (g/cm^3) ± 0.2%	T_g (K) ± 2 K	T/T_g	C_g	v	E (GPa)	H (GPa)	m	$B_{M\text{-}O}$ (kJ/mol)
$37.5MgO–12.5CaO–50.0P_2O_5$	2.53	818	0.36	0.521	0.254	63.0 ± 0.2	4.99 ± 0.03	0.0210	337.6
$50MgO–50P_2O_5$	2.44	837	0.36	0.505	0.240	55.3 ± 0.2	4.12 ± 0.02	0.0264	347.4
12.5SrO–37.5 Mg–$50.0P_2O_5$	2.66	819	0.36	0.520	0.255	62.5 ± 0.1	5.24 ± 0.02	0.0195	337.5
$25SrO–25MgO–50P_2O_5$	2.86	803	0.37	0.531	0.263	64.2 ± 0.2	5.48 ± 0.03	0.0225	327.6
$37.5SrO–12.5MgO–50.0P_2O_5$	2.95	809	0.37	0.523	0.273	61.0 ± 0.2	5.06 ± 0.04	0.0201	317.7
$50SrO–50P_2O_5$	3.18	791	0.38	0.541	0.284	55.4 ± 0.2	4.62 ± 0.02	0.0256	307.8
$12.5CaO–37.5SrO–50.0P_2O_5$	3.04	800	0.37	0.538	0.273	56.8 ± 0.2	4.71 ± 0.04	0.0224	307.9
$25CaO–25SrO–50P_2O_5$	2.92	797	0.37	0.540	0.277	58.1 ± 0.2	4.79 ± 0.03	0.0243	308.0
$37.5CaO–12.5SrO–50.0P_2O_5$	2.75	799	0.37	0.532	0.280	59.5 ± 0.2	4.86 ± 0.03	0.0201	308.0
$16.7CaO–16.7MgO–16.7SrO–50.0P_2O_5$	2.80	535	0.37	0.554	0.265	65.0 ± 0.3	5.39 ± 0.03	0.0220	321.1
$25.0CaO–12.5MgO–12.5SrO–50.0P_2O_5$	2.76	544	0.37	0.505	0.265	63.3 ± 0.3	5.21 ± 0.05	0.0219	317.9
$12.5CaO–25.0MgO–12.5SrO–50.0P_2O_5$	2.90	523	0.38	0.518	0.270	63.6 ± 0.3	5.25 ± 0.04	0.0223	327.7
$12.5CaO–12.5MgO–25.0SrO–50.0P_2O_5$	2.87	530	0.38	0.518	0.262	66.0 ± 0.3	5.52 ± 0.05	0.0232	317.8
Se [22]	4.28	314	0.93	0.852	0.322	10.3	0.36[c]	0.0909	184.2
$50Ag_2O–50P_2O_5$	4.60	435	0.69	0.520	0.376 [67,68]	24.3 ± 0.1	1.26 ± 0.01	0.0537	277.3
$45Ag_2O–45P_2O_5–10AgI$	4.85	417	0.71	0.556	0.380 [67]	23.6 ± 0.2	1.27 ± 0.02	0.0439	–
$40Ag_2O–40P_2O_5–20AgI$	5.02	403	0.74	0.586	0.381 [67]	22.6 ± 0.1	1.21 ± 0.01	0.0408	–
$35Ag_2O–35P_2O_5–30AgI$	5.10	387	0.77	0.699	0.384 [67]	20.7 ± 0.1	1.08 ± 0.01	0.0367	–
$30Ag_2O–30P_2O_5–40AgI$	5.26	366	0.82	0.624	0.389 [67]	18.6 ± 0.1	0.92 ± 0.01	0.0300	–
$25Ag_2O–25P_2O_5–50AgI$	5.53	350	0.85	0.663	0.397 [67]	16.2 ± 1.1	0.73 ± 0.08	0.0214	–
5Ge–95Se [22]	4.31	341	0.86	0.819	0.316	11.1	0.52[c]	0.0625	–
10Ge–90Se [22]	4.34	365	0.80	0.788	0.307	12.1	0.71[c]	0.0526	–
15Ge–85Se [22]	4.36	383	0.77	0.750	0.295	13.8	0.97[c]	0.0556	–
20Ge–80Se [22]	4.37	435	0.67	0.711	0.286	14.7	1.28[c]	0.0278	202.9
30Ge–70Se [22]	4.32	573	0.51	0.623	0.264	17.9	1.88[c]	0.0161	215.5
40Ge–60Se [22]	4.36	613	0.48	0.547	0.273	22.4	2.18[c]	0.0172	–
$Ce_{60}Al_{15}Cu_{10}Ni_{15}$ [69]	–	400	0.74	–	0.323 [70]	43.7	2.34	0.0160	–
$Ce_{68}Al_{10}Cu_{20}Nb_2$ [69]	–	359	0.83	–	0.328 [71]	37.1	1.69	0.0280	–
$Mg_{61}Cu_{28}Gd_{11}$ [72]	–	419	0.71	–	0.313[d]	71.6	2.94	0.0360	–
$Mg_{57.95}Cu_{26.60}Gd_{10.45}Sb_{0.05}$ [72]	–	422	0.70	–	0.313[d]	78.6	3.13	0.0220	–
$Pd_{40}Ni_{40}P_{20}$ [73]	–	576	0.51	–	0.410	102.0	6.58	0.0067	–
$Pt_{57.5}Cu_{14.7}Ni_{5.3}P_{22.5}$ [73]	–	508	0.58	–	0.390	95,0	5.08	0.0089	–
$Cu_{60}Hf_{25}Ti_{15}$ [73]	–	740	0.40	–	0.380	124.0	7.13	0.0110	–
$Zr_{55}Cu_{25}Ni_{10}Al_{10}$ [73]	–	630	0.47	–	0.330	81.0	6.01	0.0130	–
$Ni_{53}Nb_{20}Ti_{10}Zr_8Co_6Cu_3$ [73]	–	846	0.35	–	0.330	140.0	10.28	0.0120	–
$Zr_{44}Cu_{44}Al_6Ag_6$ [73]	–	718	0.41	–	0.320	100.0	6.27	0.0210	–

[a] Corning 7980 (Corning Inc.).
[b] Suprasil (Heraeus Quarglas GmbH & Co KG).
[c] Vickers hardness H_V.
[d] Poisson ratios have been chosen referring to similar compositions found in the literature [74].

3.3. Nanometric strain-rate sensitivity

The strain-rate sensitivity was studied in a strain-rate jump test as exemplarily shown in Fig. 2 for fused silica, using the same nanoindenter as described above. The employed method was originally introduced by Lucas and Oliver [23] on high-purity metallic indium. Here, we used a three-sided Berkovich diamond tip which penetrates the sample with an initial strain-rate of 0.05 s^{-1} down to 500 nm until a depth-independent hardness value is achieved [61]. With further penetration, the strain-rate is changed every 250 nm, and the hardness is determined by continuously recording the indentation depth, load and contact stiffness with the CSM equipment ($\Delta h = 5$ nm, $f = 45$ Hz). At the end of each down-jump interval, the strain-rate was switched back to the starting value of 0.05 s^{-1} which reflects in a re-increase of the hardness back to its initial value after a short transition period [23,61]. Based on the assumption of a strain-rate independent elastic modulus, the hardness from the strain-rate jump tests was calculated subsequently by combining Eqs. (5) and (7) [25,77]:

$$H = \frac{P}{A_c} = P \cdot \frac{4\beta^2}{\pi} \cdot \frac{E_r^{\,2}}{S^2} \tag{11}$$

On every sample, 10 strain-rate jump tests with strain-rates of $\dot{\varepsilon} = 0.05$; 0.007 and 0.001 s^{-1} were performed and the corresponding hardness values were averaged over the last 100 nm of each interval. It has to be noted that the nanoindenter used in this study is a load-controlled instrument. Therefore, the indentation strain-rates $\dot{\varepsilon}_i$ used in Eq. (4) to determine the strain-rate sensitivity have to be calculated from the applied strain-rates by differentiating and modifying Eq. (5) to [23]:

$$\dot{\varepsilon}_i = \frac{\dot{h}}{h} = \frac{1}{2}\left(\frac{\dot{P}}{P} - \frac{\dot{H}}{H}\right) = \frac{1}{2}\frac{\dot{P}}{P} \tag{12}$$

4. Results and discussion

In numerous studies on the indentation response of glasses, an increasing hardness with decreasing loading duration was noticed [31,58,78–85]. Although the majority of these studies had put their focus on the strain-rate dependence of the hardness, a generally accepted explanation for the origin of this effect is still missing.

4.1. Strain-rate sensitivity and reduced glass transition temperature

In earlier impression creep studies performed by Shang et al. [85] and Sakai et al. [56,57], a strong temperature-dependence in the strain-rate sensitivity of the mechanical properties of glasses has been revealed. For this reason, the influence of the temperature on the time-dependent deformation of the glasses investigated in this study was characterized at first, plotting their strain-rate sensitivity values against the reduced temperature T/T_g [86,87] (Fig. 3). Literature values from indentation creep studies on Ge–Se chalcogenide glasses [22] and various bulk metallic glasses [69,72,73] were added for comparison.

The smallest strain-rate sensitivity was determined for fused silica ($m = 0.0068$–0.0100). This result is in good agreement with previous studies [15,16,78,88], where it has already been demonstrated that fused silica does not creep significantly at room temperature, almost regardless of the applied strain-rate. As the reduced temperature increases, an increase in the strain-rate sensitivity can be observed with only the series of superionic $AgPO_3$–AgI glasses falling out of this trend. Here, the progressive substitution of $AgPO_3$ by AgI, which is accompanied by a decrease in the glass transition temperature [89,90] also results in a continuously decreasing strain-rate sensitivity. The latter is an interesting observation which can, however, be readily understood on the basis of the structure of these materials [91], as will be discussed later. The highest value of m was obtained for amorphous Se ($m = 0.0909$) [22]. Clearly, glasses become softer when approaching their glass transition temperature, i.e., with increasing T/T_g. As already noted, however, this does not necessarily result in an increase in strain-rate sensitivity. For the considered compositions, we observe an increase in m only for such glasses in whose corresponding liquids we also expect non-Newtonian flow, most prominently in vitreous Se with its structure of –Se –Se– chains [45,55]. The silver metaphosphate, on the other hand, similarly exhibits a chain-like structure of predominantly phosphate Q^2 groups, accounting for its higher value of m at ~0.7 T/T_g. The introduction of silver iodide, however, disturbs the structural predominance of phosphate chains, potentially favoring the formation of phosphate rings which are separated through the iodine groups [90]. While this decreases T_g, it also decreases the strain-rate sensitivity (even at ~0.9 T/T_g). It remains to be explored how the creation of structural anisotropy through directional flow at high load would confirm this argument. As another example, we may consider the alkaline earth metaphosphates: while they as well are dominated by Q^2 structural units with the alkaline earth (or alkali) ion more or less determining the adhesion force between the phosphate chains

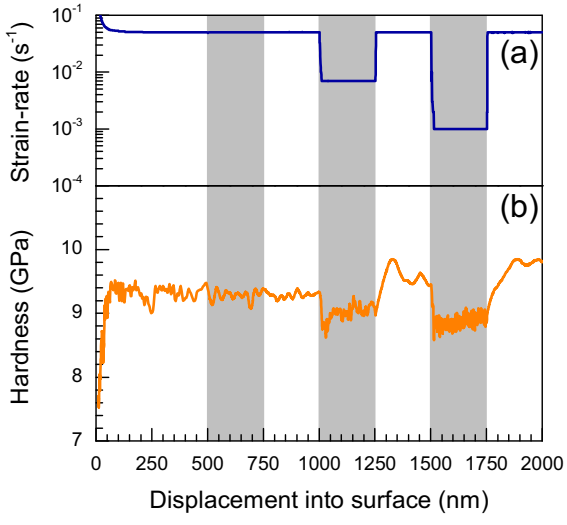

Fig. 2. Exemplary nanoindentation strain-rate jump test of fused silica (Corning 7980). (a) Applied strain-rates; (b) calculated hardness–displacement curve.

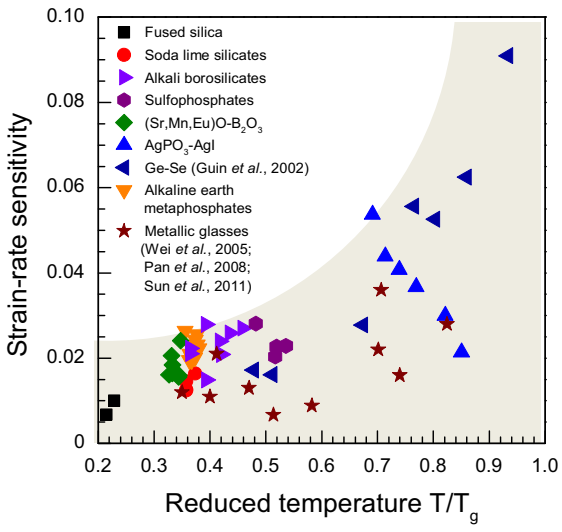

Fig. 3. Correlation between strain-rate sensitivity and reduced temperature.

[92], their strain-rate sensitivity is not notably elevated just because at the present observation temperature of ~0.4 T/T_g, we are not expecting significant viscous flow in the deformation process. Again, it remains to be explored how the value of m would change when the observation temperature approaches T_g.

An increasing creep rate with increasing temperature was reported by Sakai et al. [56,57] for fused silica, a soda-lime float glass and four other silicate glasses. Also Shang et al. [85] investigated the temperature-influence on the creep rate of a soda-lime float glass, but in contrast to the present study and the results obtained by Sakai et al., slightly higher creep rates were noticed at room temperature in comparison to the values that were determined close to the glass transition temperature. This unexpected result was attributed to the presence of adsorbed water in the room temperature indentation creep tests.

Structural water is known to enhance the indentation creep rate of glasses [58,82,93–95]. In two earlier studies, Han and Tomozawa [94] and Keulen [95] investigated the influence of the water-content on the indentation creep behavior of a sodium trisilicate and a soda-lime float glass, respectively. A considerable increase in the strain-rate sensitivity with increasing water content was found in both studies. In the present study, we make similar observations. In the series of soda-lime silicate glasses with varying water content, an increasing strain-rate sensitivity with increasing water content from $m = 0.0125$ for a glass containing 500 ppm H_2O up to $m = 0.0146$ for the same glass, but with 2000 ppm H_2O, was determined. The origin of this effect is thought to be the result of an increasing amount of non-bridging oxygen atoms inside the glass structure with the progressive water incorporation, which is accompanied by a decrease in the viscosity and therefore a significant reduction in the resistance against viscous flow [93–96]. With respect to these results the rate-dependent plastic deformation of glasses in an indentation test was assumed to be determined by inhomogeneous or non-Newtonian viscous flow [58,94,95]. In this case the increasing strain-rate sensitivity can be treated as the onset of a gradual transition from a rigid-perfectly plastic material with $m = 0$ to a linear viscous solid with $m = 1$ [41,42].

Additional support for this assumption has been given by several high-temperature indentation studies, where a gradual decrease in hardness with increasing temperature was observed [56,85–87,97–101]. Interestingly, in some of these studies a pronounced change in the hardness was noticed at temperatures exceeding $T/T_g \geq 0.7$, which was supposed to be the consequence of the increased contribution of viscous flow on the plastic deformation when approaching the glass transition [85–87,96].

Although various studies have attributed the time-dependent indentation-induced plastic deformation of glasses to the activation of non-Newtonian viscous flow, information on the flow mechanism itself are rather sparse. Nonetheless, results from high-temperature indentation studies on the plastic deformation [58,85] and crack initiation [87,97–100] in glasses have indicated that the variations in the indentation creep rates with increasing temperature can be correlated to a change in the deformation mechanism.

4.2. Strain-rate sensitivity and atomic packing density

Glasses have phenomenologically been distinguished according to their indentation response under a sharp indenter into anomalous glasses (which deform primarily through densification of the free volume) and normal glasses (which deform through localized shear flow) [7,102–104]. Indenting a normal glass with a Vickers indenter at sufficiently high load leads to the appearance of median cracks during loading and radial cracks during unloading, with the latter emanating from the corners of the residual imprint. In contrast to this, a typical crack pattern of anomalous glasses consist of ring cracks that form during loading and grow into cone cracks with further penetration of the indenter tip into the sample [103–106].

Michel et al. [100] characterized the crack initiation in fused silica at temperatures between room temperature and 673 K. In their study, the appearance of cone and radial cracks was noticed at room temperature but only radial cracks appeared at 673 K. Kurkjian et al. [98] investigated the crack morphologies of fused silica and of a soda-lime silicate glass at room temperature and at 77 K. At room temperature, the soda-lime silicate glass exhibited the typical normal indentation behavior with the formation of four radial cracks at the corners of the residual imprint. On the contrary, when indenting the same sample at 77 K, no radial cracks were visible. The influence of the temperature on the plastic deformation of a soda-lime silicate glass was also characterized by Shang et al. [58,85]. In their studies, a significantly higher contribution of shear flow to plastic deformation was noticed as the temperature increases. Considering these observations, it has been assumed that the variation in the indentation creep rate with increasing temperature is governed by the transition from a glass which mainly densifies under load towards more and more shear-mediated plastic deformation [56,58,85,98].

Indentation experiments [102,107], compression studies [108,109] and theoretical calculations [110] have shown that the capability of a glass to densify under external pressure depends on the amount of free volume inside the glass network. Based on the above, an increase in the atomic packing density (a decrease in the molar free volume) can therefore lead to a higher indentation creep rate. To now evaluate potential implications of this argument for the rate dependence of hardness, the atomic packing densities of all glasses investigated in this study were calculated and correlated with the corresponding values of strain-rate sensitivity.

The atomic packing density C_g is defined as the theoretical molar volume of the atoms divided by the effective molar volume of the glass [111]:

$$C_g = \rho \frac{\sum f_i V_i}{\sum f_i M} \tag{12}$$

In the above equation $V_i = 4/3\pi N(xr_A^3 + yr_B^3)$ is the molar volume of an oxide A_xB_y with the molar fraction f_i, the molar mass M_i and the density ρ and the Avogadro constant N. The ionic radii r_A and r_B of the corresponding cations and anions were taken from Shannon [112]. Since the atoms in Ge–Se chalcogenides are covalently bound [113–115], the covalent radii were used in place of the ionic radii of Ge^{4+} and Se^{2-} in those glasses.

In Fig. 4 the strain-rate sensitivity is plotted over the atomic packing density. Consistent with the previous discussion, the smallest value for m was found for fused silica which is known to densify by as much as 20% under isostatic pressure [116–118]. For the other oxide and chalcogenide glasses, a rough trend is visible where an increase in the atomic packing density is accompanied by an increase in the *variability* of strain-rate sensitivity: a stronger variation of strain-rate sensitivity from very low to very high is found with increasing packing density. This indicates that at moderate or high packing density ($C_g > 0.5$), other parameters are dominating the strain-rate dependence of hardness. The highest values of m are found in the Ge-Se chalcogenide glass system, where plastic deformation proceeds over localized shear [108,119,120]. More generally, we may speculate that the probability of finding a (localized) shear band in a disordered system increases with increasing packing density, as also the degree of order increases. This assumption apparently holds even in oxide glasses, where evidence for shear band formation has been observed under high pressure [36].

Again, an interesting example is provided by the series of superionic $AgPO_3$–AgI glasses. Here, the increase in the atomic packing density with increasing AgI concentration is accompanied by a decrease in the strain-rate sensitivity. As noted before, this observation can readily be understood on the basis of a structural consideration. $AgPO_3$ consists of long chains of corner-sharing $[PO_4]^{3-}$ tetrahedra. The non-bridging

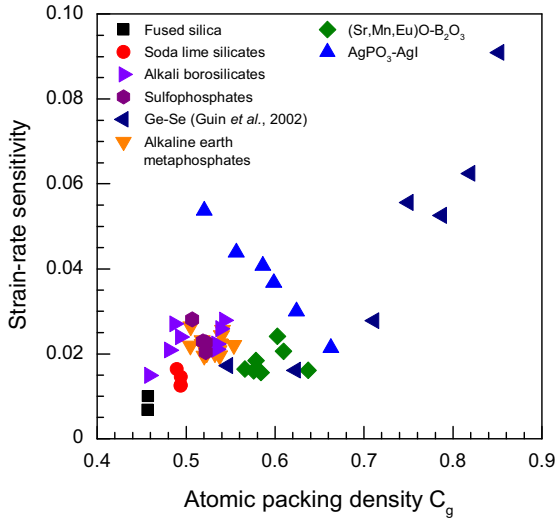

Fig. 4. Correlation between strain-rate sensitivity and atomic packing density of glasses.

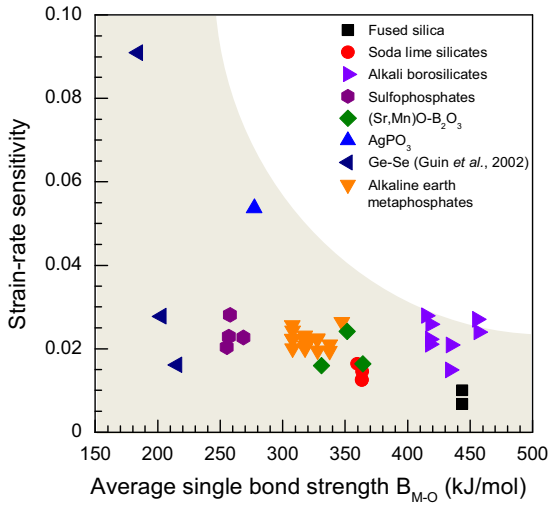

Fig. 5. Correlation between the average single bond strength and the strain-rate sensitivity of glasses.

oxygens are charge-compensated by the Ag^+ ions, whereas the formation of weak Ag–O ionic bonds leads to a cross-linking between the phosphate chains [89,121]. With the incorporation of AgI, the spacing between these chains increases, enabling the conduction of the Ag^+ ions [121,122]. This decreases the rate dependence of deformation, even though it increases the degree of packing.

It is interesting to note that the largest variations in the strain-rate sensitivity occur in the Ge–Se chalcogenide glass system. At low germanium concentrations Ge–Se chalcogenide glasses consist primarily of selenium chains and eight-membered selenium rings. Plastic deformation is assumed to proceed over the alignment of the selenium chains in shear planes (as noted before). The resistance against shear is quite small and originates only from weak inter-chain Van der Waals forces. However, the progressive addition of germanium creates cross-links between the selenium chains, leading to an increasing shear resistance [54,115,119]. Therefore, it appears that the significant drop in strain-rate sensitivity from $m = 0.0909$ for amorphous selenium down to $m = 0.0172$ for $Ge_{40}Se_{60}$ [22] is not only based on the atomic packing density, but that also the network dimensionality plays an important role.

4.3. Strain-rate sensitivity and bond strength

In contrast to Ge–Se chalcogenides, shear deformation in oxide glasses is partially reconstructive and involves the breaking and formation of new bonds [103,108,123]. It is assumed that shear flow is favored along the weak ionically bound interfaces in network modifier-rich regions [98,105,123]. The influence of the average single bond strength on the mechanical properties of oxide glasses has already been observed by Mackenzie et al. [6,124,125] To validate the magnitude of this effect on the strain-rate sensitivity, the average single bond strength B_{M-O} was calculated by summing-up the single bond strengths of the individual constituents weighted by their molar fraction f_i [125]:

$$B_{M-O} = \sum f_i \cdot \frac{E_d}{N_{A-B}}, \tag{13}$$

According to Sun [126] the single bond strength can be derived from the dissociation energy E_d of a simple oxide A_xB_y into the gaseous atoms divided by the oxygen coordination number of the cation N_{A-B} in the corresponding glass. The dissociation energies for a variety of oxides can be found in the literature [127].

In Fig. 5, we plot the strain-rate sensitivity against the average single bond strength of the considered glasses. The values for amorphous Se, $Ge_{20}Se_{80}$ and $Ge_{30}Se_{70}$ were added for comparison. For the latter, the single bond strengths of $B_{Ge-Ge} = 157$ kJ/mol, $B_{Ge-Se} = 215$ kJ/mol and $B_{Se-Se} = 184$ kJ/mol were taken from Nguyen et al. [128]. Considering Fig. 5, the average single bond strength seems to have little or no effect on the strain-rate sensitivity of oxide glasses. This reflects in the similar strain-rate sensitivities of all glasses over a very large difference in average single bond strength, ranging from sulfophosphates and alkaline earth metaphosphates to alkali borosilicate glasses. Although on a low absolute level, marked variations in the strain-rate sensitivity were also found for glasses with average single bond strengths of the same magnitude, such as fused silica of varying quality and some alkali borosilicates. On the other hand, in the Ge–Se glass system, plastic deformation does not involve the breakage of bonds [129]. In fact, as already noted, the mechanical properties of this system are governed by the degree of inter-chain cross-linking.

4.4. Strain-rate sensitivity and Poisson ratio

Earlier calculations done by Makishima and Mackenzie [124] had shown that the Poisson ratio correlates-well with the atomic packing density. This correlation has later been confirmed through experimental data for a variety of glass systems [111]. Meanwhile, the Poisson ratio is often used as an indicator for the mechanism which underlies the permanent deformation of a glass. It was found that the amount of densified volume in an indentation hardness test can be estimated by annealing the indented sample for 2 h at a reduced temperature of $T/T_g = 0.9$ [7,9,130,131]. With this method a pronounced contribution of localized shear flow on plastic deformation could be verified for glasses with high Poisson ratios [131,132]. Apart from this, Rouxel [111] also reported a relation between the Poisson ratio and the network dimensionality of a glass, where a high network connectivity is accompanied by a low Poisson ratio. On the other hand, a low degree of cross-linking leads to high Poisson ratios.

Following these arguments, the strain-rate sensitivity is plotted against the Poisson ratio in Fig. 6. We observe an increase in the *variability* of the strain-rate sensitivity with increasing Poisson ratio up to $\nu \sim 0.33$. For higher Poisson ratios, this variability decreases again. That is, for the observed range of compositions, glasses with a Poisson ratio in the ~0.3–0.4 range exhibit a wide range of the degree of loading-rate dependence of local deformation. This is a surprising observation on the first glance, but may be explained through a consideration of the structural properties which govern plastic deformation: with decreasing dimensionality of the network, we may – up to a certain degree – expect an increasing contribution from shear-mediated

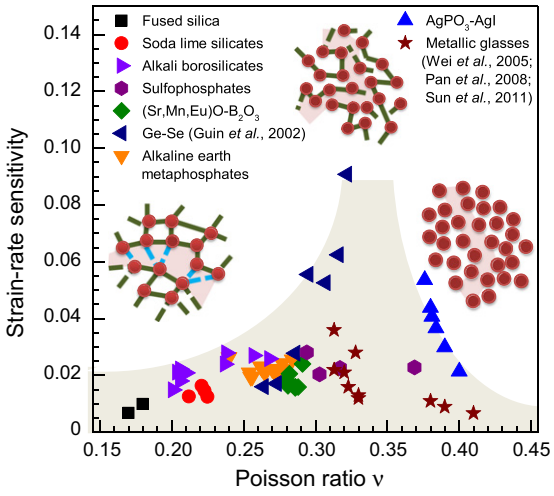

Fig. 6. Correlation between Poisson ratio and the strain-rate sensitivity of glasses. The insets represent three general types of glass structures (from left to right): a three-dimensional network which is determined primarily by bond strength, a complex low-dimensional structure, and an arrangement which is dominated by packing density. The highlighted regions in the three arrangements show hypothetic shear regions.

deformation, which may result in some small if any rate dependence of hardness. However, at low Poisson ratio (high network dimensionality and low packing density), we assume that the limiting factor in deformation would primarily be the network connectivity or bond strength: once an activation barrier is overcome, deformation is only weakly loading-rate-dependent. This is regardless of the height of the activation barrier. In analogy, at high Poisson ratio (low network dimensionality and high packing density), once a shear plane is found by the system, deformation proceeds virtually loading-rate independent. Only in the intermediate region where neither bond strength nor packing density alone limits plastic deformation, the specific structural (and chemical) arrangement of the system plays a major role in the strain-rate sensitivity. That is, for intermediate network dimensionality, a very large variation of strain-rate sensitivity with Poisson ratio can be obtained through varying the structural complexity of the system. In this sense, we would speculate that the highest strain-rate sensitivity would occur for a pure chain structure with very weak inter-chain bonding.

With this result not only the large variations in the time-dependent deformation of the Ge–Se chalcogenide glasses can be explained. Also the increased strain-rate sensitivity of silicate glasses at high water concentrations which was observed in this study (as well as in previous investigations [94,95]), is assumed to originate from the reduced network connectivity. These findings give additional support to the hypothesis that the rate-dependent plastic deformation of at least oxide and chalcogenide glasses proceeds over localized shear. The series of superionic $AgPO_3$–AgI glasses again confirms this trend. Here, the incorporation of AgI (already found to decrease the strain-rate sensitivity), leads to an increase in the Poisson ratio [67,68]. The origin of this behavior is still unclear to us, but may be related to the occurrence of fast deformation which is mediated by the highly mobile inter-chain Ag^+ species. Such fast deformation would lead to an apparent decrease in the strain-rate sensitivity.

5. Conclusions

In summary, we investigated the loading-rate dependence of plastic deformation in inorganic glasses over a wide range of packing densities and average single bond strengths. We have shown that the strain-rate jump test, performed through instrumented nanoindentation, is a suitable method to determine the local strain-rate sensitivity of disordered materials within a single experiment. Through relating the strain-rate sensitivity to various structural properties of the glass, we arrive at the following conclusions:

- Clearly, the strain-rate sensitivity is not related to softness or plasticity of a material, but it is determined by the multitude of structural parameters which present a kinetic barrier to plastic deformation.
- While glasses become softer when approaching their glass transition temperature, this does not necessarily result in increasing strain-rate sensitivity. That is, high values of m at $T/T_g \geq 0.7$ where observed only in such glasses where inhomogeneous or non-Newtonian viscous flow is expected also in the corresponding liquid. Vice versa, such glasses do not necessarily exhibit high m at low T/T_g.
- Strain-rate sensitivity does not strongly correlate with packing density or bond strength. However, a larger variability of strain-rate sensitivity is obtained only at intermediate values of both parameters. This indicates that such cases, other parameters such as chemical composition and specific structural arrangement are dominating the strain-rate dependence of hardness. On the other side, for high bond strength and connectivity or for high packing density, the strain-rate sensitivity of the considered glasses is always low.
- The latter is *in line* with the dependence of strain-rate sensitivity on Poisson ratio, where we observe a strong increase in the variability of the strain-rate sensitivity at $\nu \sim 0.33$. For higher or lower Poisson ratios, the value of m is always low (within the considered range of compositions). That is, for the observed range of compositions, glasses with a Poisson ratio of ~0.3–0.4 exhibit a wide range of the degree of loading-rate dependence of local deformation. At lower or higher Poisson ratio, we assume that the limiting factor in deformation is primarily network connectivity and bond strength or packing density, respectively: once an activation barrier is overcome, deformation is only weakly loading-rate-dependent. This is regardless of the height of the activation barrier.
- Small strain-rate sensitivities were found for glasses with a highly cross-linked network and a large amount of molar free volume, whereas high strain-rate sensitivities were found for glasses with intermediate network connectivity and a high atomic packing density. Considering these results, the loading-rate-dependent plastic deformation of glasses with higher T_g relative to the observation temperature is supposed to be the result of localized shear flow. The increase of the strain-rate sensitivity with increasing atomic packing density and decreasing network dimensionality, respectively, can therefore be attributed to a transition from an anomalous glass, that mainly deforms through compaction of the free volume, to a normal glass, where the plastic deformation proceeds over shear flow along the weak ionically bonded interfaces in the network modifier-rich regions. Nonetheless, it has to be noted that this general conclusion is not applicable to all glass systems, as also the network topology plays an important role. One example for such a deviation is given through the series of silver metaphosphate-silver iodide glasses, which comprise a marked chain structure with adjustable inter-chain distance. Here, hardness, strain-rate sensitivity, packing density and Poisson ratio can be tuned adversely through the incorporation of intermediate network constraints.

Acknowledgments

Financial support by the German Science Foundation through its priority program SPP 1594 (project no. WO 1220/10-1) is gratefully acknowledged. The authors wish to thank all colleagues at the Laboratory of Glass Science at the Otto Schott Institute of Materials Science, University of Jena for providing the glass samples. We further thank Dominique de Ligny, Institut Lumière Materière, University of Lyon 1, Lyon, France for performing Brillouin scattering experiments.

References

[1] L. Wondraczek, J.C. Mauro, J. Eckert, U. Kuhn, J. Horbach, J. Deubener, T. Rouxel, Adv. Mater. 23 (2011) 4578–4586.
[2] E.W. Taylor, Nature 163 (1949) 323-323.
[3] J. Sehgal, S. Ito, J. Non-Cryst. Solids 253 (1999) 126–132.
[4] J.C. Sangleboeuf, T. Rouxel, Indentation and scratching of glass: load, composition environment and temperature effects, in: R.C. Bradt, D. Munz, M. Sakai, K.W. White (Eds.), Fracture Mechanics of Ceramics, Springer Science + Business Media, Inc., New York, NY, 2005, pp. 121–133.
[5] G.R. Anstis, P. Chantikul, B.R. Lawn, D.B. Marshall, J. Am. Ceram. Soc. 64 (1981) 533–538.
[6] M. Yamane, J.D. Mackenzie, J. Non-Cryst. Solids 15 (1974) 153–164.
[7] J.E. Neely, J.D. Mackenzie, J. Mater. Sci. 3 (1968) 603–609.
[8] K.I. Nomura, Y.C. Chen, R.K. Kalia, A. Nakano, P. Vashishta, Appl. Phys. Lett. 99 (2011) 111906 (1–3).
[9] S. Yoshida, J.C. Sangleboeuf, T. Rouxel, J. Mater. Res. 20 (2005) 3404–3412.
[10] J. Hay, Exp. Tech. 33 (2009) 66–72.
[11] J. Mencik, Meccanica 42 (2007) 19–29.
[12] W.C. Oliver, G.M. Pharr, J. Mater. Res. 7 (1992) 1564–1583.
[13] X.D. Li, B. Bhushan, Mater. Charact. 48 (2002) 11–36.
[14] B. Wolf, Cryst. Res. Technol. 35 (2000) 377–399.
[15] T. Chudoba, F. Richter, Surf. Coat. Technol. 148 (2001) 191–198.
[16] A.C. Fischer-Cripps, Mater. Sci. Eng. A 385 (2004) 74–82.
[17] Y.T. Cheng, C.M. Cheng, Mater. Sci. Eng. R 44 (2004) 91–149.
[18] I.C. Choi, B.G. Yoo, Y.J. Kim, J.I. Jang, J. Mater. Res. 27 (2012) 2–10.
[19] W.D. Nix, H.J. Gao, J. Mech. Phys. Solids 46 (1998) 411–425.
[20] P. Grau, G. Berg, H. Meinhard, S. Mosch, J. Am. Ceram. Soc. 81 (1998) 1557–1564.
[21] S.N.G. Chu, J.C.M. Li, J. Mater. Sci. 12 (1977) 2200–2208.
[22] J.P. Guin, T. Rouxel, V. Keryvin, J.C. Sangleboeuf, I. Serre, J. Lucas, J. Non-Cryst. Solids 298 (2002) 260–269.
[23] B.N. Lucas, W.C. Oliver, Metall. Mater. Trans. A 30 (1999) 601–610.
[24] L. Shen, W.C.D. Cheong, Y.L. Foo, Z. Chen, Mater. Sci. Eng. A 532 (2012) 505–510.
[25] V. Maier, B. Merle, M. Göken, K. Durst, J. Mater. Res. 28 (2013) 1177–1188.
[26] C.J. Su, E.G. Herbert, S. Sohn, J.A. LaManna, W.C. Oliver, G.M. Pharr, J. Mech. Phys. Solids 61 (2013) 517–536.
[27] A.A. Elmustafa, S. Kose, D.S. Stone, J. Mater. Res. 22 (2007) 926–936.
[28] A. De La Torre, P. Adeva, M. Aballe, J. Mater. Sci. 26 (1991) 4351–4354.
[29] V. Raman, R. Berriche, J. Mater. Res. 7 (1992) 627–638.
[30] F.Q. Yang, J.C.M. Li, Mater. Sci. Eng. R 74 (2013) 233–253.
[31] H. Meinhard, P. Grau, G. Berg, S. Mosch, Glass Sci. Technol. 70 (1997) 333–339.
[32] L. Wondraczek, H. Behrens, J. Chem. Phys. 127 (2007) 154503 (1–10).
[33] S. Fuhrmann, T. Deschamps, B. Champagnon, L. Wondraczek, J. Chem. Phys. 140 (2014) 054501 (1–7).
[34] A. Winterstein-Beckmann, D. Möncke, D. Palles, E.I. Kamitsos, L. Wondraczek, J. Non-Cryst. Solids 401 (2014) 110–114.
[35] L. Wondraczek, S. Sen, H. Behrens, R.E. Youngman, Phys. Rev. B 76 (2007) 014202 (1–9).
[36] S.K. Lee, P.J. Eng, H.K. Mao, Y. Meng, M. Newville, M.Y. Hu, J.F. Shu, Nat. Mater. 4 (2005) 851–854.
[37] A. Vegiri, E.I. Kamitsos, Phys. Rev. B 82 (2010) 054114 (1–9).
[38] D. Tabor, Rev. Phys. Technol. 1 (1970) 145–179.
[39] L. Kogut, K. Komvopoulos, J. Mater. Res. 19 (2004) 3641–3653.
[40] Z. Song, K. Komvopoulos, Mech. Mater. 61 (2013) 91–100.
[41] A.F. Bower, N.A. Fleck, A. Needleman, N. Ogbonna, Proc. R. Soc. Lond. A 441 (1993) 97–124.
[42] R. Goodall, T.W. Clyne, Acta Mater. 54 (2006) 5489–5499.
[43] A. Juhász, P. Tasnádi, P. Szászvári, I. Kovács, J. Mater. Sci. 21 (1986) 3287–3291.
[44] M.J. Mayo, R.W. Siegel, A. Narayanasamy, W.D. Nix, J. Mater. Res. 5 (1990) 1073–1082.
[45] M. Cukierman, D.R. Uhlmann, J. Non-Cryst. Solids 12 (1973) 199–206.
[46] J.H. Li, D.R. Uhlmann, J. Non-Cryst. Solids 3 (1970) 127–147.
[47] J.H. Simmons, R.K. Mohr, C.J. Montrose, J. Appl. Phys. 53 (1982) 4075–4080.
[48] S.L. Webb, D.B. Dingwell, Phys. Chem. Miner. 17 (1990) 125–132.
[49] R. Brückner, Y.Z. Yue, J. Non-Cryst, J. Non-Cryst. Solids 175 (1994) 118–128.
[50] J.H. Simmons, R. Ochoa, K.D. Simmons, J.J. Mills, J. Non-Cryst, J. Non-Cryst. Solids 105 (1988) 313–322.
[51] G. Cseh, N.Q. Chinh, P. Tasnádi, P. Szommer, A. Juhász, J. Mater. Sci. 32 (1997) 1733–1739.
[52] C. Bernard, V. Keryvin, J.C. Sangleboeuf, T. Rouxel, Mech. Mater. 42 (2010) 196–206.
[53] C.Y.S. Chang, W.C.J. Wei, C.H. Hsueh, J. Non-Cryst. Solids 357 (2011) 1414–1419.
[54] Y. Gueguen, T. Rouxel, P. Gadaud, C. Bernard, V. Keryvin, J.C. Sangleboeuf, Phys. Rev. B 84 (2011) 064201 (1–10).
[55] W.H. Poisl, W.C. Oliver, B.D. Fabes, J. Mater. Res. 10 (1995) 2024–2032.
[56] M. Sakai, S. Shimizu, J. Non-Cryst. Solids 282 (2001) 236–247.
[57] M. Sakai, S. Shimizu, S. Ito, J. Am. Ceram. Soc. 85 (2002) 1210–1216.
[58] H.X. Shang, T. Rouxel, J. Am. Ceram. Soc. 88 (2005) 2625–2628.
[59] F.Q. Yang, J.C.M. Li, J. Non-Cryst. Solids 212 (1997) 136–142.
[60] P. Manns, R. Brückner, Glastech. Ber. 61 (1988) 46–56.
[61] V. Maier, K. Durst, J. Mueller, B. Backes, H.W. Höppel, M. Göken, J. Mater. Res. 26 (2011) 1421–1430.
[62] J. Alkorta, J.M. Martínez-Esnaola, J.G. Sevillano, Acta Mater. 56 (2008) 884–893.
[63] N. Da, O. Grassme, K.H. Nielsen, G. Peters, L. Wondraczek, J. Non-Cryst. Solids 357 (2011) 2202–2206.
[64] A. Winterstein-Beckmann, D. Moncke, D. Palles, E.I. Kamitsos, L. Wondraczek, J. Non-Cryst. Solids 376 (2013) 165–174.
[65] J.P. Malugani, A. Wasniewski, M. Doreau, G. Robert, A. Alrikabi, Mater. Res. Bull. 13 (1978) 427–433.
[66] B. Martin, L. Wondraczek, J. Deubener, Y.Z. Yue, Appl. Phys. Lett. 86 (2005) 121917 (1–4).
[67] R. Bogue, R.J. Sladek, Phys. Rev. B 42 (1990) 5280–5288.
[68] L. Börjesson, S.W. Martin, L.M. Torell, C.A. Angell, Solid State Ionics 18–19 (1986) 431–436.
[69] B.C. Wei, T.H. Zhang, W.H. Li, D.M. Xing, L.C. Zhang, Y.R. Wang, Mater. Trans. 46 (2005) 2959–2962.
[70] J. Fornell, S. Surinach, M.D. Baro, J. Sort, Intermetallics 17 (2009) 1090–1097.
[71] B. Zhang, D.Q. Zhao, M. Pan, R.J. Wang, W.H. Wang, Acta Mater. 54 (2006) 3025–3032.
[72] Y.D. Sun, Z.Q. Li, J.S. Liu, M.Q. Cong, J.Y. Qin, J. Rare Earth 29 (2011) 253–258.
[73] D. Pan, A. Inoue, T. Sakurai, M.W. Chen, Proc. Natl. Acad. Sci. U. S. A. 105 (2008) 14769–14772.
[74] X.K. Xi, R.J. Wang, D.Q. Zhao, M.X. Pan, W.H. Wang, J. Non-Cryst. Solids 344 (2004) 105–109.
[75] G.M. Pharr, W.C. Oliver, F.R. Brotzen, J. Mater. Res. 7 (1992) 613–617.
[76] N.A. Sakharova, J. Fernandes, J.M. Antunes, M.C. Oliveira, Int. J. Solids Struct. 46 (2009) 1095–1104.
[77] D.L. Joslin, W.C. Oliver, J. Mater. Res. 5 (1990) 123–126.
[78] A.A. Elmustafa, D.S. Stone, J. Mater. Res. 22 (2007) 2912–2916.
[79] T. Rouxel, J.C. Sangleboeuf, C. Moysan, B. Truffin, J. Non-Cryst. Solids 344 (2004) 26–36.
[80] R. Chakraborty, A. Dey, A.K. Mukhopadhyay, Metall. Mater. Trans. A 41A (2010) 1301–1312.
[81] M. Yoshioka, N. Yoshioka, J. Appl. Phys. 78 (1995) 3431–3437.
[82] S.P. Gunasekera, D.G. Holloway, Phys. Chem. Glasses 14 (1973) 45–52.
[83] C.J. Fairbanks, R.S. Polvani, S.M. Wiederhorn, B.J. Hockey, B.R. Lawn, J. Mater. Sci. Lett. 1 (1982) 391–393.
[84] R.J. Anton, G. Subhash, Wear 239 (2000) 27–35.
[85] H.X. Shang, T. Rouxel, M. Buckley, C. Bernard, J. Mater. Res. 21 (2006) 632–638.
[86] T. Watanabe, Y. Benino, T. Komatsu, J. Non-Cryst. Solids 286 (2001) 141–145.
[87] E. Le Bourhis, T. Rouxel, J. Non-Cryst. Solids 316 (2003) 153–159.
[88] Y.I. Golovin, A.I. Tyurin, V.V. Khlebnikov, Tech. Phys. 50 (2005) 479–483.
[89] D.L. Sidebottom, Phys. Rev. B 61 (2000) 14507–14516.
[90] D.I. Novita, P. Boolchand, M. Malki, M. Micoulaut, J. Phys. Condens. Matter 21 (2009) 205106 (1–17).
[91] B.P. Rodrigues, L. Wondraczek, J. Chem. Phys. 138 (2013) 244507 (1–5).
[92] R.K. Brow, J. Non-Cryst. Solids 263 (2000) 1–28.
[93] K. Hirao, M. Tomozawa, J. Am. Ceram. Soc. 70 (1987) 497–502.
[94] W.T. Han, M. Tomozawa, J. Am. Ceram. Soc. 73 (1990) 3626–3632.
[95] N.M. Keulen, J. Am. Ceram. Soc. 76 (1993) 904–912.
[96] R.F. Bartholomew, J. Non-Cryst. Solids 56 (1983) 331–342.
[97] E. Le Bourhis, D. Metayer, J. Non-Cryst. Solids 272 (2000) 34–38.
[98] C.R. Kurkjian, G.W. Kammlott, M.M. Chaudhri, J. Am. Ceram. Soc. 78 (1995) 737–744.
[99] M.D. Michel, A. Mikowski, C.M. Lepienski, C.E. Foerster, F.C. Serbena, J. Non-Cryst. Solids 348 (2004) 131–138.
[100] M.D. Michel, F.C. Serbena, C.M. Lepienski, J. Non-Cryst. Solids 352 (2006) 3550–3555.
[101] J.H. Westbrook, Phys. Chem. Glasses 1 (1960) 32–36.
[102] K.W. Peter, J. Non-Cryst. Solids 5 (1970) 103–115.
[103] A. Arora, D.B. Marshall, B.R. Lawn, M.V. Swain, J. Non-Cryst. Solids 31 (1979) 415–428.
[104] R.F. Cook, G.M. Pharr, J. Am. Ceram. Soc. 73 (1990) 787–817.
[105] J.T. Hagan, M.V. Swain, J. Phys. D 11 (1978) 2091–2102.
[106] B.R. Lawn, M.V. Swain, J. Mater. Sci. 10 (1975) 113–122.
[107] P. Sellappan, T. Rouxel, F. Celarie, E. Becker, P. Houizot, R. Condradt, Acta Mater. 61 (2013) 5949–5965.
[108] T. Rouxel, H. Ji, J.P. Guin, F. Augereau, B. Ruffle, J. Appl. Phys. 107 (2010) 094903 (1–5).
[109] T. Rouxel, H. Ji, T. Hammouda, A. Moreac, Phys. Rev. Lett. 100 (2008) 225501 (1–4).
[110] E.H. Yoffe, Philos. Mag. A 46 (1982) 617–628.
[111] T. Rouxel, J. Am. Ceram. Soc. 90 (2007) 3019–3039.
[112] R.D. Shannon, Acta Crystallogr. A 32 (1976) 751–767.
[113] E. Gulbrandsen, H.B. Johnsen, M. Endregaard, T. Grande, S. Stolen, J. Solid State Chem. 145 (1999) 253–259.
[114] P.S. Salmon, J. Non-Cryst. Solids 353 (2007) 2959–2974.
[115] U. Senapati, A.K. Varshneya, J. Non-Cryst. Solids 185 (1995) 289–296.
[116] H.M. Cohen, R. Roy, Phys. Chem. Glasses 6 (1965) 149–161.
[117] J.D. Mackenzie, J. Am. Ceram. Soc. 46 (1963) 461–470.
[118] S. Susman, K.J. Volin, D.L. Price, M. Grimsditch, J.P. Rino, R.K. Kalia, P. Vashishta, G. Gwanmesia, Y. Wang, R.C. Liebermann, Phys. Rev. B 43 (1991) 1194–1197.
[119] J.P. Guin, T. Rouxel, J.C. Sangleboeuf, I. Melscoet, J. Lucas, J. Am. Ceram. Soc. 85 (2002) 1545–1552.
[120] J.C. Mauro, A.K. Varshneya, J. Am. Ceram. Soc. 90 (2007) 192–198.
[121] J.D. Wicks, L. Börjesson, G. Bushnellwye, W.S. Howells, R.L. Mcgreevy, Phys. Rev. Lett. 74 (1995) 726–729.
[122] J. Swenson, L. Börjesson, Phys. Rev. Lett. 77 (1996) 3569–3572.
[123] F.M. Ernsberger, J. Non-Cryst. Solids 25 (1977) 293–321.
[124] A. Makishima, J.D. Mackenzie, J. Non-Cryst. Solids 17 (1975) 147–157.

[125] A. Makishima, J.D. Mackenzie, J. Non-Cryst. Solids 12 (1973) 35–45.
[126] K.H. Sun, J. Am. Ceram. Soc. 30 (1947) 277–281.
[127] K.H. Sun, M.L. Huggins, J. Phys. Colloid Chem. 51 (1947) 438–443.
[128] V.Q. Nguyen, J.S. Sanghera, I.D. Aggarwal, I.K. Lloyd, J. Am. Ceram. Soc. 83 (2000) 855–859.
[129] D.R. Swiler, A.K. Varshneya, R.M. Callahan, J. Non-Cryst. Solids 125 (1990) 250–257.
[130] J.D. Mackenzie, J. Am. Ceram. Soc. 46 (1963) 470–476.
[131] S. Yoshida, S. Isono, J. Matsuoka, N. Soga, J. Am. Ceram. Soc. 84 (2001) 2141–2143.
[132] Y. Kato, H. Yamazaki, S. Yoshida, J. Matsuoka, J. Non-Cryst. Solids 356 (2010) 1768–1773.